Chemical Science

MINIREVIEW

View Article Online
View Journal | View Issue

Cite this: *Chem. Sci.*, 2018, **9**, 4370

Recent advances in near-infrared II fluorophores for multifunctional biomedical imaging

Feng Ding,†[a] Yibei Zhan,†[b] Xiaoju Lu†[b] and Yao Sun *[a]

Received 12th March 2018
Accepted 19th April 2018

DOI: 10.1039/c8sc01153b

rsc.li/chemical-science

In recent years, owing to unsatisfactory clinical imaging clarity and depths in the living body for early diagnosis and prognosis, novel imaging modalities with high bioimaging performance have been actively explored. The remarkable headway made in the second near-infrared region (NIR-II, 1000–1700 nm) has promoted the development of biomedical imaging significantly. NIR-II fluorescence imaging possesses a number of merits which prevail over the traditional and NIR-I (400–900 nm) imaging modalities in fundamental research, such as reduced photon scattering, as well as auto-fluorescence and improved penetration depth. Functional probes for instant and precise feedback of *in vivo* information are at the core of this modality for superb imaging. Herein, we review the recently developed fluorophores including carbon nanotubes, organic small molecules, quantum dots, conjugated polymers and rare-earth-doped materials to present superior and multifunctionality of biomedical imaging in the NIR-II regions (1000–1700 nm).

Introduction

Modern biomedical imaging techniques are essential tools in clinical diagnosis and therapy assessment, allowing the non-invasive, highly sensitive and specific observation of pathological and physiological events associated with human diseases in living subjects.[1–4] For the past few decades, a diversity of imaging modalities, such as fluorescence imaging (FI), photoacoustic imaging (PI), positron emission tomography (PET) and magnetic resonance imaging (MRI), combined with promising probes, have been well developed and greatly expedited the prosperity of bioimaging in preclinical and clinical practice.[5–15] Among these modalities, fluorescence imaging in the first near-infrared region (NIR-I; 700–900 nm, Fig. 1a) has received considerable attention in biomedical research owing to its high sensitivity, quick feedback, non-hazardous radiation, low cost, and so forth.[16–26] For instance, NIR-I fluorophores utilizing rational design strategies have been widely used for biomedical applications such as accurate real-time sentinel lymph nodes/tumor delineation, as well as intraoperative image-guided surgical removal of sentinel lymph nodes/tumor tissues.[27–29] Fluorophores with emissions in the NIR-I region can achieve deeper penetration and superior imaging qualities compared to those with visible wavelengths.[30,31] Moreover, recent studies suggest that fluorescence imaging at the second near-infrared region (NIR-II, 1000–1700 nm) can give a better fluorescence image quality and signal-to-background ratios (SBR) than at the NIR-I region.[4,32] Significant improvements in the imaging temporal and spatial resolution (~20 ms and ~25 μm) and penetration depth (up to ~3 cm) have been fulfilled by this innovative NIR-II region in biomedical imaging, due to the reduced scattering, negligible tissue absorption and minimum

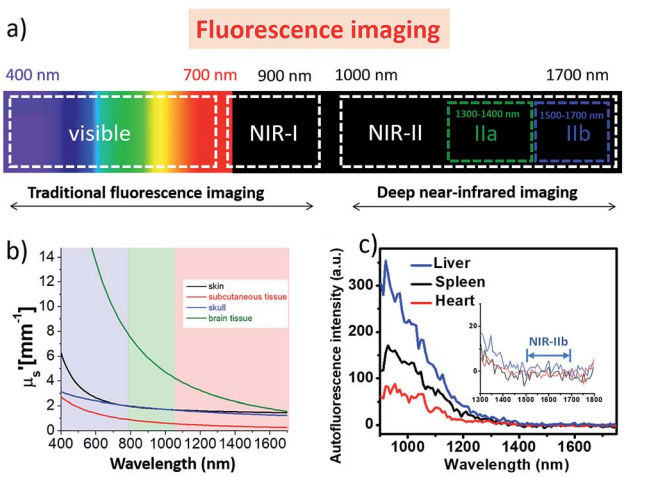

Fig. 1 (a) Wavelengths for fluorescence imaging; (b) the reduced scattering coefficient, μs, is plotted as a function of wavelength in the range of 400–1700 nm for various tissue types including the skin (black), the brain tissue (green), the skull (blue) and the subcutaneous tissue (red). (c) Auto-fluorescence spectrum of *ex vivo* mouse liver, spleen and heart tissue.

[a]*Key Laboratory of Pesticides and Chemical Biology, Ministry of Education, International Joint Research Center for Intelligent Biosensor Technology and Health, Hubei International Scientific and Technological Cooperation Base of Pesticide and Green Synthesis, Chemical Biology Center, College of Chemistry, Central China Normal University, Wuhan 430079, China. E-mail: sunyaogbasp@mail.ccnu.edu.cn*

[b]*School of Chemistry and Chemical Engineering, Hubei Polytechnic University, Hubei, 435003, China*

† These authors contributed equally to this work.

auto-fluorescence (Fig. 1b and c).[33,34] The pioneering work of *in vivo* NIR-II fluorescence imaging began with the utilization of carbon nanotubes.[34] Since then, several other available fluorophores, including small organic dyes,[35,36] quantum dots[37,38] conjugated polymers[39] and rare-earth-doped nanoparticles,[40] have also been actively employed for NIR-II biomedical imaging. This article aims to cover the recently reported NIR-II fluorophores and highlight their multifunctional biomedical applications in the NIR-II region.

Single-walled carbon nanotubes for NIR-II imaging

The small size and unique structure of single-walled carbon nanotubes (SWCNTs) dictate their promising mechanical, electronic, physical and chemical properties. This has constantly motivated the discovery of their potentials in various scientific fields, in particular in biomedical imaging.[33,41–44] SWCNTs are quasi 1-D quantum wires with sharp densities of electronic states (electronic DOS) at the van Hove singularities, conferring appealing optical features.[43] The unique band gap and large stoke shift of SWCNTs make them ideal candidates as fluorophores for bioimaging.[33,45] SWCNTs generally absorb photons in the NIR-I region (700–900 nm) and emit fluorescence in the range of 800 nm to 2000 nm which mostly fall under the NIR-II region (1000–1700 nm), enabling a deep-tissue penetration and high spatial resolution fluorescence imaging.[33,43,46] However, SWCNTs suffer from the issues of poor solubility and biocompatibility, and this is responsible for the limitation of the direct use of hydrophobic SWCNTs in bioimaging. To address these issues, several chemical approaches, including noncovalent and covalent surface modification, have been used to functionalize the surface of SWCNTs.[47–51] Despite the fact that the covalent modification strategy has been widely adopted by many groups to improve the solubility and biocompatibility of SWCNTs, this has always damaged the conjugated π network and caused surface defects, which leads to weak fluorescence imaging performance and decreased fluorescence quantum yield.[33] Noncovalent modification strategies meant that the possibly of the notorious disturbance to both the architecture and the NIR-II fluorescence properties of SWCNTs could be avoided.[52] However, noncovalent methods such as PEGylation ordinarily induced a drastic discount in the quantum yield (QY). In particular, Dai's group provided a pivotal breakthrough to endow SWCNTs with solubility, biocompatibility and a high QY for versatile biological applications by dispersing SWCNT in sodium cholate and subsequently displacing the disperse medium with phospholipid-polyethylene glycol (PL-PEG).[34]

Thus, the functionalized SWCNTs were reported as promising fluorophores for cell NIR-II imaging on account of their high photostability and good biocompatibility.[53,54] The cell NIR-II fluorescent imaging can not only track the distribution of intracellular SWCNTs, but also observe the interactions between SWCNTs and biomolecules.[55,56] Based on these precedent studies, Dai's group demonstrated an example of tumor specific target HER2 receptors for BT-474 cells imaging *via* the conjugation of PEGylated SWCNTs with Herceptin.[57] After this, Dai's group also implemented SWCNTs as a first generation NIR-II fluorophore for *in vivo* fluorescence imaging of living objects, which opens up the possibility of using SWCNTs to visualize the vascular network with deeper tissue penetration, and a higher temporal and spatial resolution (<300 ms, ~10 μm) in the NIR-II region.[34] With the development of these brightly fluorescent and biocompatible SWCNTs, a number of applications such as high-performance imaging of blood flow dynamics, tracking of the whole-body blood circulation and lymphatic system and guidance for tumor surgery have been achieved.[58–61] Despite these favorable results, due to being hampered by the thick skull, the high resolution and quick feedback imaging of small vessels and dynamic blood flow in the brain has remained a great challenge to current imaging modalities. Fortunately, the discovery of larger-diameter SWCNTs and a transition shift to longer wavelengths in the NIR-IIb window (1500–1700 nm) could provide the clear-cut advantages of negligible scattering, zero endogenous tissue auto-fluorescence and unparalleled tissue-imaging depths.[62] Dai's group recently evaluated the non-invasive fluorescence imaging at a depth of ~3 mm through the intact scalp and skull of C57B1/6 mice in the NIR-IIb region by injection with SWCNTs.[62] Compared with the obscure cerebrovascular structures in the NIR-I and NIR-II regions, the sharper cerebral capillaries with a greater fidelity and higher SBR in the NIR-IIb region exhibited in the brain imaging implied a prodigious potential for future diagnosis and monitoring of brain diseases (Fig. 2).

Meanwhile, NIR-II brain imaging was also explored to identify the hemodynamic difference between a healthy brain and a brain with the cerebral arterial occlusion (MCAO) model of stroke.[63] NIR-II images apparently revealed the fluorescence signal significantly reduced the cortical blood perfusion in the left cerebral hemisphere of the mouse associated with the cerebral artery, whereas it was intact for the normal mouse (Fig. 3a–i). However, SWCNTs currently synthesized for bioimaging typically involve various chiralities, and each of them corresponds to diverse excitation and emission wavelengths, and the reduced availability of SWCNTs excited by a laser weakens the fluorescent intensity.[64] Although dielectrophoresis, density gradient centrifugation, DNA wrapping chromatography and gel filtration are

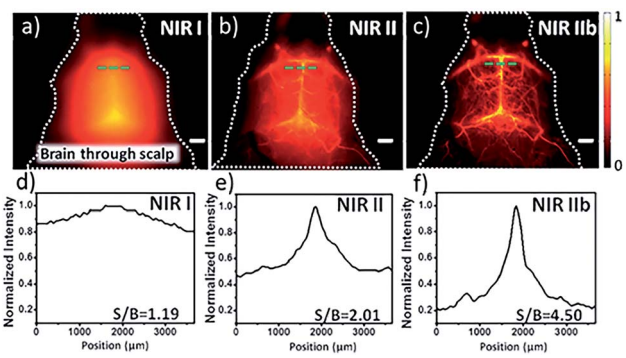

Fig. 2 Fluorescence imaging of the cerebrovasculature of mice without craniotomy in the (a) NIR-I; (b) NIR-II and (c) NIR-IIb regions, with the corresponding SBR analysis shown in (d)–(f). Scale bars: 2 mm. Reproduced from ref. 62 with permission from John Wiley and Sons.

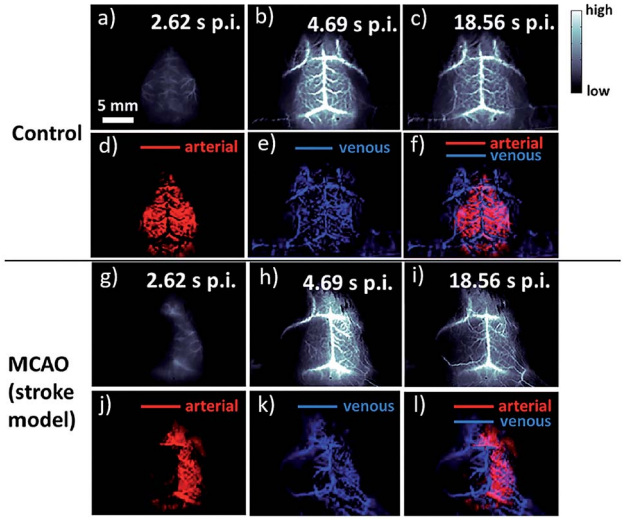

Fig. 3 Fluorescence imaging of the cerebrovasculature of mice without craniotomy. (a)–(c) Time-course NIR-IIa images of a control healthy mouse (mouse C1); (d)–(f) PCA overlaid images showing arterial (red) and venous (blue) vessels of mouse C1. (g)–(i) Time-course NIR-IIa images of a mouse with MCAO (mouse M1); (j)–(l) PCA overlaid images showing arterial (red) and venous (blue) vessels of mouse M1. Scale bars: 2 mm. Reproduced from ref. 63 with permission from Springer Nature.

actively applied to separate mixed chiral SWCNTs, there is still room to achieve maximum separation efficiency.[65–68] NIR-II fluorescent imaging with SWCNTs has indicated tremendous superiorities in biomedical imaging, which surpass other classical imaging techniques. The future fundamental research should focus on increasing the QY and purifying chiralities of SWCNTS to enhance fluorescent intensity and acquire multicolored NIR-II fluorescence imaging. Being the first of the NIR-II fluorophores, the utilization of SWCNTs for *in vitro* and *in vivo* bioimaging has stimulated the search for other inorganic and organic agents in the NIR-II region.

Small-molecule organic fluorophores for NIR-II imaging

So far, nanoparticles have captured increasing attention because of their excellent characteristics for NIR-II imaging. Nevertheless, most current nanoparticle based fluorophores are excreted slowly and mainly retained in the liver and spleen.[4,69] In contrast, small-molecule organic fluorophores are exceptional candidates for clinical imaging and are widely known for their desirable features such as rapid metabolism, low toxicity and well-defined architectures.[36,70–72] However, the concept of small-molecule based NIR-II fluorophores is simple, the procedure of design and synthesis is a tricky problem for organic chemists, which means that the development of small-molecule NIR-II dyes lies far behind that of their nanoparticle-based counterparts.[72,73] Fortunately, the significant progress made in material science, including organic infrared LEDs, organic solar cells and organic electronics has provided some inspiration to chemists.[74–76] In addition, the donor–acceptor (D–A) architecture has been widely applied for small molecular NIR-I probes, and the combination of strong electron donors and acceptors could lower the energy gap resulting in several NIR-I probes with an emission wavelength near ~900 nm.[74] Encouraged by this result, the introduction of a second strong donor in the D–A scaffold could form symmetrical donor–acceptor–donor (D–A–D) architectures. Based on this D–A–D scaffold, the spatial configuration of strong electron-donating groups flanking a central electron acceptor serves to shrink the energy gap separating the hybridized highest occupied molecular orbital (HOMO)/lowest unoccupied molecular orbital (LUMO) levels and drives the fluorescence emission into the NIR-II window.[4] Recently, with this rational design, Dai, Cheng and Hong reported the first generation of D–A–D type small-molecule NIR-II organic fluorophores: CH1055 (970 Da, maximum emission at 1055 nm) for NIR-II *in vivo* biomedical imaging.[36] The PEGylated CH1055 exhibited outstanding properties for *in vivo* pharmacokinetics and more than 90% of the CH1055 was fast excreted through the renal system within 24 h (Fig. 4a). In the following study, both the brain vasculature and orthotropic glioblastoma brain tumors could be efficiently detected with high resolution at a depth of ~4 mm in the brain (Fig. 4b and c). Successively, tumor-targeted molecular imaging and precise image-guided surgery were performed by means of the conjugation of CH1055 to a targeting ligand (anti-EGFR affibody) and displayed a superior SBR of 15 (Fig. 4d). These promising results highlighted CH1055 as a generic NIR-II reporter for extensive use in future NIR-II bioimaging.

The D–A–D scaffold is the key to achieving organic fluorophores with emission wavelengths longer than 1000 nm in NIR-II region, and the combination of various spacers (thiophene), electron donors (fluorene and triphenylamine) and central electron accepting aromatic backbones (benzobisthiadiazole, BBTD) could greatly expand the library of small-molecule NIR-II fluorophores. However, the complex and

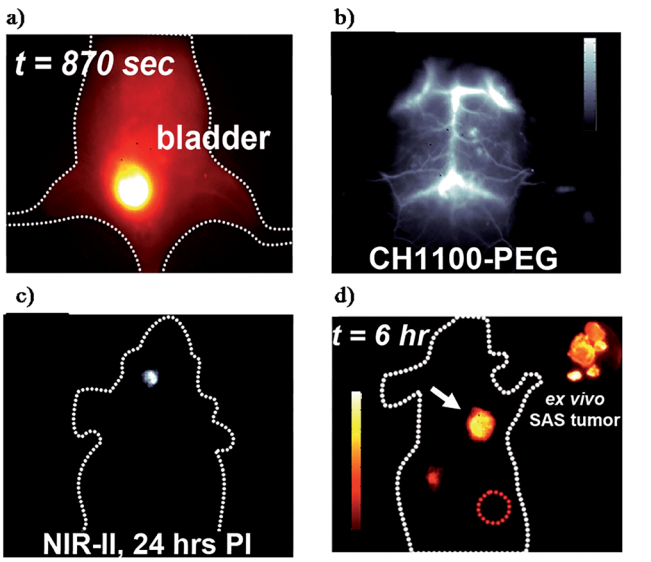

Fig. 4 (a) Renal excretion of CH1055-PEG. (b) Brain vessel imaging. (c) Glioblastoma brain tumor detection. (d) Molecular imaging of skin cancer tumors *via* the CH1055-affibody. Reproduced from ref. 36 with permission from Springer Nature.

multiple synthetic steps with low yields and tedious chromatographic isolation are still the chief chemical impediments to broaden the comprehension and boost facile preparations of small-molecular based NIR-II fluorophores. Faced with these challenges, Hong's group recently reported a collection of feasibly fabricated NIR-II fluorophores: Q1, Q4 and H1 (Fig. 5).[77–79] It should be pointed out that all of these small-molecule NIR-II fluorophores were hydrophobic intrinsically and could not be used directly for *in vivo* applications. To solve this problem, diverse chemical approaches have been used, including tailoring these fluorophores with polyethylene glycol (PEG) or targeted peptides/affibodies or encapsulating them in hydrophilic polymer matrixes, fortunately, these have proven to give decent outcomes.[36,77–79]

The first case of an actively targeted NIR-II probe, SCH1100, was designed based on the conjugation of Q4 to a RM26 peptide (a gastric-releasing peptide receptor targeting ligand), bringing about bright NIR-II specific fluorescent imaging of prostate cancer *in vivo*.[77] Based on a Q4 scaffold, the dynamic monitoring of the angiogenesis of the tumor with high resolution in the NIR-II region was accomplished facilely. In practice, selectively removing part of the sentinel lymph nodes (SLNs) can alleviate the symptoms of lymphedema that would be triggered by total lymph node removal, which could contribute to preventing the emergence of cancer metastasis. However, the lack of effective techniques always stands in the way of an ideal clinical practice. Here, the SLNs were successfully identified, even when covered with soft tissue, and precisely resected under the assistance of H1 encapsulated into an amphipathic phospholipid-PEG shell (H1NPs), which supplied a promising tool for SLNs removal.[78] Meanwhile, a high-performance NIR-II probe: CQS1000, produced from Q1 could noninvasively provide real-time monitoring of arterial thrombus formation and ischemia with high spatial and temporal resolution.[79] Despite all these benefits from NIR-II imaging, the fluorescence QY is less than 0.30% in aqueous solutions and remains the major bottleneck for these organic fluorophores.[80]

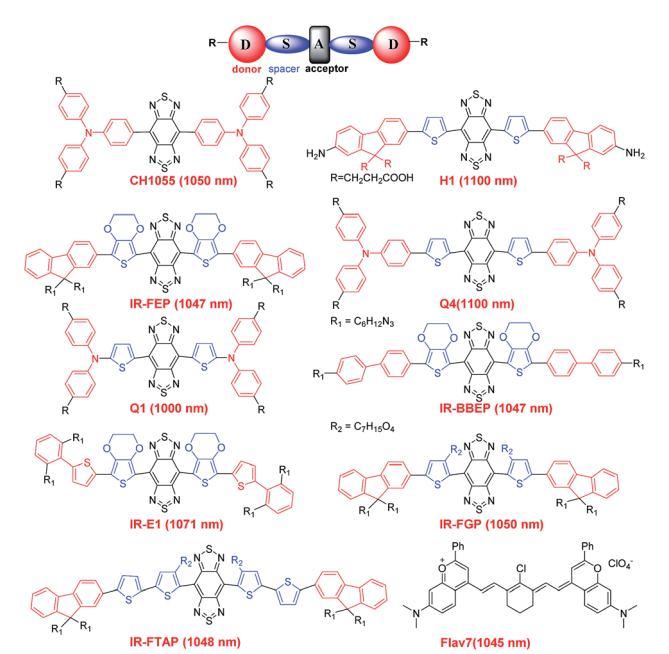

Fig. 5 The library of small organic NIR-II fluorophores.

In fact, the generally low QYs of these NIR-II fluorophores in aqueous media seems to be highly related to the interactions with H_2O molecules.[81,82] In order to enhance the QY, Dai and Liang's group introduced a shielding unit (S) to the D–A–D scaffold and the side chains of the shielding units extend out of the conjugated backbone, excluding the continuous intermolecular interactions.[82–85] Moreover, the utilization of a 3,4-ethylenedioxy thiophene (EDOT) donor, replacing thiophene, could manifestly increase the quantum yield.[82,83] Thus, several optimized NIR-II organic fluorophores based on the S–D–A–D–S scaffold with improved fluorescent characteristics have been established and the elevated fluorescence brightness facilitated multifunctional NIR-II bioimaging, such as dynamic vascular changes in a traumatic brain injury mouse model and multicolor molecular 3D imaging of histological brain tissues.[82–85] Recently, thiophene has been ushered in as the second donor connected to this S–D–A–D–S scaffold and the obtained IR-FTAP has been described as having one of the highest QY, with 5.3% for the molecular NIR-II fluorophore in aqueous solutions.[86] Meanwhile, Dai's group conjugated an IR-FEP-based fluorophore: 3,4-ethylenedioxythiophene polyethylene-glycol carboxyl (IR-FEPC) to human chorionic gonadotropin (hCG) to prepare bioconjugates which gave superb 3D imaging, specifically of ovaries.[87] Furthermore, Cosco *et al.* engineered rational modifications on cyanine dyes by replacing the indolenines heterocycles with dimethyl-flavylium heterocycles and the resulting dyes have been used to visualize deep vasculature in a mouse.[71] To further accelerate the clinical use of new NIR-II imaging techniques, the utilization of ICG, a FDA-approved small-molecule fluorophore, has also been extended for bioimaging in the NIR-II region and showed an unexpected imaging performance.[88,89] In addition, a surge in dual modal instrumentation development for clinical applications has sparked the discovery of more dual modal probes to clearly delineate the localization and expression of biochemical markers, and effectively track the tumors with high-resolution and high-sensitivity.[90–92] For example, a powerful synergy can be achieved by combining PET imaging for localization of tumors in the whole body without penetration limitations, and NIR-II imaging for subsequent precise delineation of tumor lesions and resection margins.[93,94] Recently, Hong's group reported the first NIR-II/PET dual-modal RGD peptide-based probe and achieved precise tumor delineation and image-guided surgery.[95] Taking into account the accessible clinical translation, small-molecule NIR-II fluorophores are still considered to be encouraging candidates due to their rapid renal or hepatic metabolism. There are several chemical and optical properties of small molecule fluorophores that should be optimized, such as the small molecular weight (<500 Da), good aqueous solubility (beyond the PEG modification), facile and controllable decorations, simple synthetic strategies, high quantum yield and long emission wavelength (>1500 nm).

Quantum dots for NIR-II imaging

Quantum dots (QDs) are colloidal semiconductor nanocrystals, they absorb light and generate excitons simultaneously in the nanocrystals, and the electron–hole recombination induces luminescence. A great majority of QDs are constructed as core/shell structures with the core nanocrystal overcoated with another semiconductor material to guard and enhance the optical properties.[96] The broad excitation spectrum, narrow emission spectrum, high quantum yield and high resistance to photo-bleaching of QDs leads to a notable bioimaging performance *in vivo* with a high spatial and temporal resolution, and they are catching great interest.[97] Unlike carbon nanotubes, QDs such as PbS, CdSe, Ag_2S and so forth can be finely tuned in size and shape to modulate pharmacokinetics and tissue distribution.[98–101] Recently, Ag_2S dots coated with six-armed PEG demonstrated the first case of fluorescent imaging of xenograft tumors through a pronounced permeability and retention effect in the NIR-II region.[37] More importantly, the Ag_2S dots exhibited a dramatically higher QY (15% *vs.* 0.5% for carbon nanotubes) and stability than previously described NIR-II fluorophores.[37,102] As the *in vivo* real-time dynamic visualization of the circulatory system can deepen the understanding of tumorigenesis and metastasis, PEGylated Ag_2S dots have been explored to image the circulatory system including lymphatic monitoring, blood flow and angiogenesis mediated by tumors with high SBR (Fig. 6).[103] Ag_2S dots also offer the possibility of dynamically tracking the fate of the transplanted human mesenchymal stem cells (HMSCs) in living animals. The HMSCs labeled with Ag_2S dots did not interfere with stem cell proliferation and the dynamic process of the migration and distribution of HMSCs in response to the chemotactic factor SDF-1α on the cutaneous wound and the healing effect was visualized *in situ*.[103,104] Recently, protein nanocage (PNC) encaged Ag_2S dots achieved real-time tracking of *in vivo* immigration behavior of PNC and the interaction between the PNC and host body, which could prompt the development of future protein-based drug delivery systems.[105]

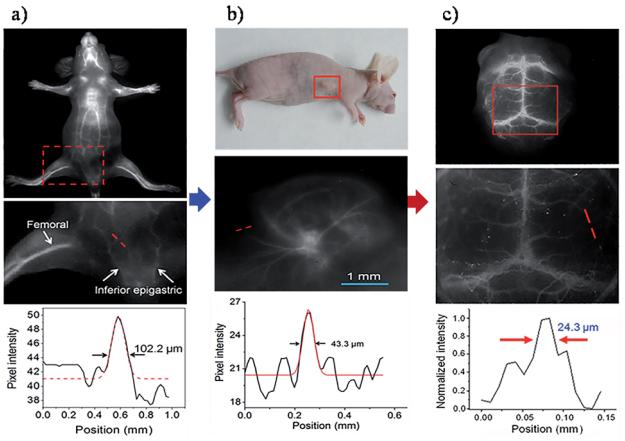

Fig. 6 (a) Blood vascular imaging of a nude mouse with PEGylated Ag_2S QDs. (b) Imaging of U87MG tumor blood vascular with PEGylated Ag_2S QDs. (c) NIR-II images of the vasculature of brain. Reproduced from Ref. 102 with permission from Elsevier Ltd.

In addition to Ag_2S dots, PbS dots seemed to be more attractive candidates for NIR-II imaging, which can be ascribed to the higher QY and longer emission wavelength.[101] However, the toxicity of lead heavily confined the applications *in vivo*. Aiming to increase the biocompatibility, glutathione and protein have been utilized for PbS dots coating, yet the fluorescence quenching when exposed to water is another problem.[100,106] An excellent quantum yield of 17% was achieved by the design of PbS@CdS core–shell QDs and the emission wavelengths could be expediently regulated from 1000 nm to 1500 nm by changing the core diameter.[107] Based on these promising results, this NIR-II agent can image blood vasculature in the brain with high fidelity. Furthermore, PbS@CdS was surface-functionalized with SiO_2 and an amphiphilic polymer (pluronic F-127) coating, contributing to a dual-layer protection for the PbS@CdS core and stabilizing the resulting PbS@CdS@SiO_2@F-127 NPs in an extremely acidic (pH = 1–4) and alkaline (pH = 10–13) environment. Furthermore, these types of nanoparticles displayed superior brain vessel imaging with a penetration depth up to 950 μm and decent gastrointestinal (GI) tract imaging.[108] More recently, a class of high-performance and high QY (30%) indium–arsenide-based QDs have been engineered and focused for unprecedented applications, such as quantifying the breathing and heartbeat rates in awake and unrestrained animals and plotting three-dimensional quantitative flow maps of the mouse brain vasculature.[109] Undoubtedly, QDs are considered to be exceptional alternatives amongst the fluorescent dyes. Reasonable strategies to further increase the QY of QDs and lengthen the emission wavelength are driving forces to elaborate powerful tools to solve existing and up-coming challenges in biochemical studies. As QDs are being investigated for wide ranging bioimaging purposes, mounting the desirable optical properties of QDs will be elicited with the evolution of QDs and derivatives based on QDs.

Conjugated polymers and rare-earth-doped materials for NIR-II imaging

The design of conjugated polymers generated through D–A alternating copolymerization provided an effective way of synthesizing polymers with tunable bandgap energy in the NIR-I and NIR-II regions.[110–114] It is reported that a more electron-donating donor and more electron-withdrawing acceptor can generally achieve a smaller band gap in the copolymer. In addition, a longer copolymer results in a reduced band gap with a greater delocalization of π-electrons.[115,116] Recently, based on the D–A structure, Hong *et al.* reported a brightly NIR-II fluorescent copolymer (poly(benzo[1,2-*b*:3,4-*b*′]difuran-*alt*-fluorothieno-[3,4-*b*]thiophene)), pDA, Fig. 7a.[39] The water soluble and biocompatible pDA-based NIR-II probes were fabricated through a non-covalently functionalized PEGylated surfactant with emission at ~1050 nm and a high QY (~1.7% *vs.* ~0.4% for carbon nanotubes) (Fig. 7b–d). Molecular targeted imaging of the epidermal growth factor receptors (EGFRs) on the tumor cell membranes was achieved by cetuximab conjugated pDA-PEG. The results of the cell imaging confirmed that the pDA-PEG

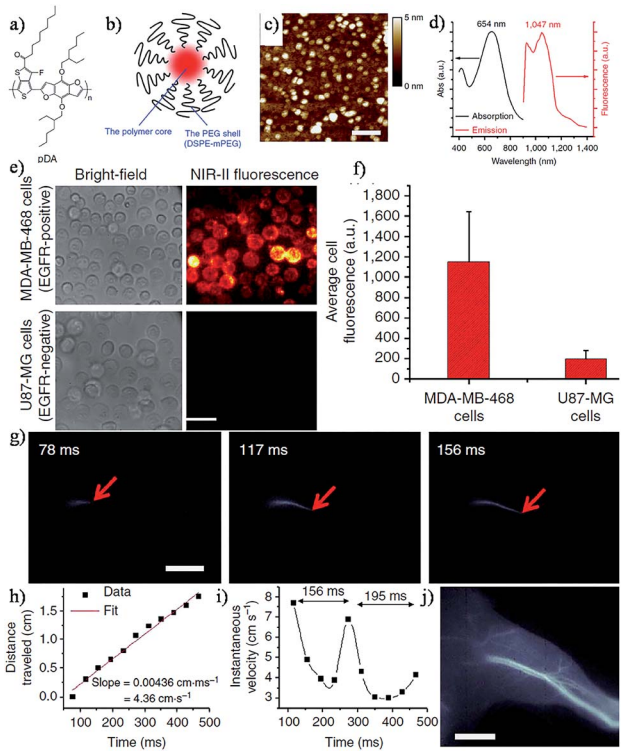

Fig. 7 (a) The structure of the pDA polymer. (b) The schematic of the pDA-PEG nanoparticle based NIR-II probe. (c) AFM image of the pDA-PEG probe. (d) Absorption and emission spectra of pDA-PEG; (e) white-light and NIR-II images of EGFR-positive MDA-MB-468 cells and EGFR-negative U87MG cells incubated with the pDA-PEG-Erbitux conjugate. (f) Average NIR-II fluorescence of EGFR-positive MDA-MB-468 cells and EGFR-negative U87MG cells, showing a positive/negative ratio of 5.8. (g) A time course of NIR-II fluorescence images of a mouse hindlimb immediately following intravenous injection of pDA-PEG. (h) A plot of the distance travelled by the blood flow front as a function of time. The linear fit reveals an average blood velocity of 4.36 cm s^{-1} in the femoral artery. (i) A plot of instantaneous velocity (derived by dividing flow front travelled distance between two consecutive frames by the time interval of 39 ms) as a function of time, revealing periodic changes of instantaneous velocity corresponding to cardiac cycles. (j) An NIR-II fluorescence image of the same mouse hindlimb after full perfusion of pDA-PEG-containing blood into the hindlimb, upon which the fluorescence intensity in the hindlimb became unchanging. The scale bars in (g) and (j) indicate 5 mm. Reproduced from ref. 39 with permission from Springer Nature.

based NIR-II probe was capable of recognizing and staining tumor cells specifically (Fig. 7e–f). Furthermore, it can dynamically provide an ultrafast image and track real-time arterial blood flow when the pDA-PEG based probe enters the mouse hindlimb (Fig. 7g). More recently, Shou *et al.* reported diketopyrrolopyrrole-based semiconducting polymer nanoparticles for *in vivo* NIR-II imaging of tumors in a subcutaneous osteosarcoma model, and assessment of vascular embolization therapy of tumors and NIR-II image-guided tumor surgery.[117] For a wider application of conjugated polymers, manipulation of the critical D–A structure of polymers will enable more desirable electronic and optical properties, such as tuning of the emission wavelength to achieve a deeper penetration *in vivo* and a higher resolution, and may promote the progress of biomedical imaging based on the platform of conjugated polymers.

The rare-earth (RE)-doped nanoparticles (RENPs), known for their specific luminescence, have gained continuing attention in recent years in biomedical applications due to their minimal photo bleaching, excellent tunable emission wavelength, long luminescence lifetime and superior photostability by doping host materials with diverse RE metal ions.[118–120] REs always emit fluorescence by NIR-induced upconversion phosphorescence. Upconversion is an anti-stokes process that relates to the absorption of two or more low energy NIR photons (typically 980 nm) by REs, while an emission of one higher energy photon is in the visible range.[121] Commonly, they are prepared as core–shell particles with the core consisting of the host material and dopants, and the undoped host material encasing the core structure as a shell. The shell in this structure cannot only keep the dopants from degradation, but also decrease the quenching effects in surfaces and strengthen fluorescence actions.[122] With the fourteen rare-earth elements furnishing different energy level transitions, REs can permit a wide range of emission profiles by selecting the appropriate dopant(s).[123–126] However, conventional biomedical imaging using RENPs has mainly been concerned with detecting the NIR-I emissions, largely putting aside the NIR-II emissions generated simultaneously upon excitation.[120,126] Fortunately, the distinctively optical properties of RENPs in the NIR-II region were unearthed and employed for visualizing biological information *in vivo*.[126–128] Naczynski *et al.* demonstrated the first example of tumor detection using multispectral NIR-II imaging (NIR-IIa, ~1185 nm and NIR-IIb, ~1525 nm) with $NaYF_4$Yb:Ln (Ln: Er, Ho, Tm or Pr) nanoprobes (REs), and Er-doped nanoparticles were proved to be the brightest SWIR-emitting RE-doped phosphors.[129] By modification of REs with FDA-approved albumin, they were able to obviously improve the bioactivity of the REs NIR-II probes, such as enhanced REs accumulation at tumors and outstanding *in vivo* pharmacokinetics.[127] Although the NIR-IIb emission has exemplified the enhanced resolution of vasculature structures in the mouse, a relatively low QY of RENPs in toluene and ease of quenched after transferring to aqueous solutions are still problems for bioimaging.[130,131] To deal with these matters, Zhong *et al.* recently designed a RENPs with high QY and emission at ~1550 nm *via* the installation of a 2% Er and Ce co-doped $NaYbF_4$ core and an inert $NaYF_4$ shell for NIR-IIb imaging (Fig. 8a and b).[132] Owing to the Ce doping, the pathway of up-conversion efficiency decreased while down-conversion increased by nine times (Fig. 8c). Ultimately, by general van der Waals interactions between the alkyl chains of poly(maleic anhydride-*alt*-1-octadecene) (PMH) and the oleic acid molecules, a hydrophilic polymer shell was formed to afford a decent dispersibility and stability in aqueous solutions (Fig. 8d). After a further PEGylation step, Er-RENPs@PMH-PEG gave an outstanding biocompatibility performance (Fig. 8e and f). Benefiting from the high-performance luminescence of the Ce doped Er-RENPs, dynamic imaging and tracking of arterial blood flow in the mouse brain in the NIR-IIb window with high-resolution exhibited a much shorter exposure time (20 ms) than previous rare-earth materials, carbon nanotubes and QD based NIR-II probes. Due to the decent photostability and long

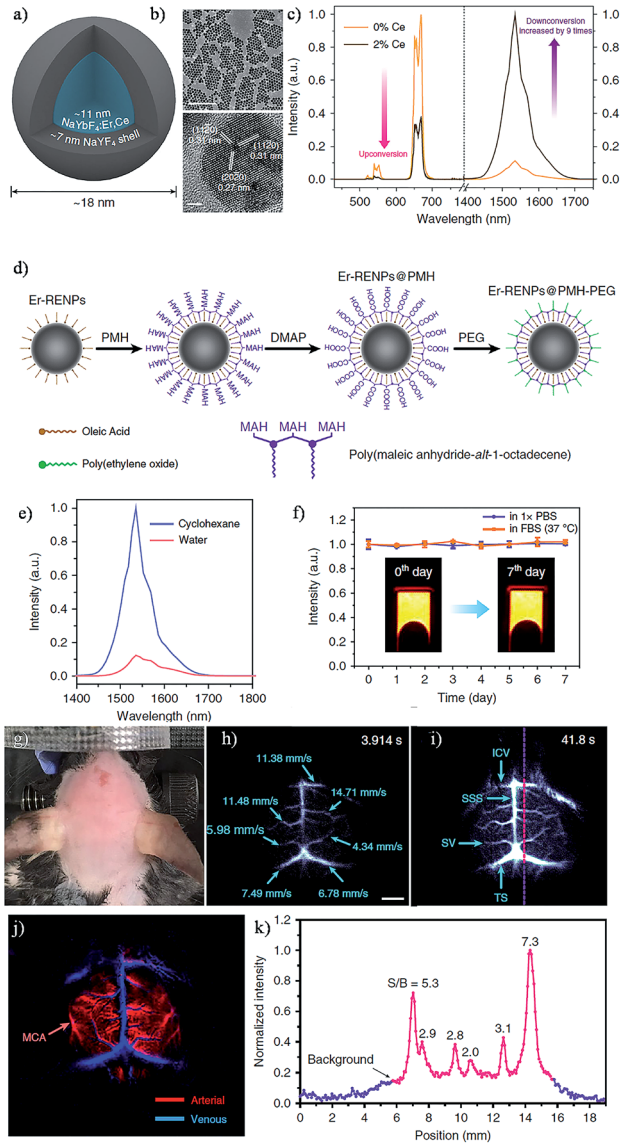

Fig. 8 (a) Schematic design of a Ce^{3+} doped Er-RENPs. (b) TEM and HRTEM images. (c) The luminescence spectrum of the Er-RENPs with or without 2% Ce^{3+} doping. (d) Schematic illustration outlining the surface modification of the Er-RENPs. (e) The luminescence spectrum of oleic acid-capped Er-RENPs dispersed in cyclohexane and Er-RENPs@PMH-PEG dispersed in water. (f) The photostability of Er-RENPs@PMH-PEG in PBS and FBS solutions. (g) Color photograph of a C57Bl/6 mouse. (h) and (i) time-course NIR-IIb brain fluorescence images showing the perfusion of RENPs into various cerebral vessels. (j) Cerebral vascular image in the NIR-IIb region with corresponding PCA overlaid image. (k) SBR analysis of the NIR-IIb cerebrovascular image. Reproduced from ref. 132 with permission from Springer Nature.

term luminescence of REs, the future of REs in biomedical imaging is evidently promising. However, due to the immense hindrance of latent danger for living subjects, repeated evaluation of the clearance and toxicity of REs are still crucial to further confirm the availability of REs in clinical studies. Thus, the next generation REs should be developed with reliable quantitation which can reduce the biotoxicity by controlling the dose for use and create a deeper tissue molecular imaging.

Conclusions and perspectives

Overall, we have outlined multiple superiorities of NIR-II fluorophores which can be attributed to self-excellent optical properties and the introduction of the NIR-II region into biomedical imaging, such as low auto-fluorescence, high spatial and temporal resolution, and deep organs and tissues penetration. Also, the NIR-II fluorophores with versatile properties aforementioned are capable of diversifying bio-imaging applications, which could render specific tools aimed at particular bioimaging practices. Herein, we envisage a promising future considering the following points.

Although the successes made by NIR-II fluorophores have enriched our understanding and the applications in the NIR-II bioimaging field, current studies have mainly focused on basic research, which means that there is still a long way to go before their application in clinic studies. One of the concerns is that the biotoxicity may be bred from the complex physiological functions in human body. Furthermore, deficiencies of NIR-II dyes, such as optical properties with low QY and short emission wavelength, chemical synthesis with tedious and time-consuming synthesis steps, and bio-applications with poor biocompatibility, seriously hinder the clinical translation. In addition to removing the above impediments through rational strategies, entire preclinical procedures for NIR-II dyes to evaluate the activity, toxicology and pharmacokinetics in animal models are of paramount importance for human molecular imaging in the NIR-II window.

Secondly, a high-performance NIR-II fluorophore with a smart design has the possibility to greatly expand the applications from molecular imaging to chemical biology and analytic chemistry. For example, the non-invasive and dynamic visualization of the interactions between small molecule–protein, protein–protein, or DNA–protein with high temporal and spatial resolution at a living subject level is urgently demanded for chemical biology. The utilization of small-molecule NIR-II fluorophores labelled with these molecules could afford better spatial resolution, sensitivity and deeper tissue penetration in live animals, which would help to clarify indefinite biochemical mechanisms.[133–135] Moreover, the currently NIR-II probes are not always directly associated with specific interactions to targets of interest and may not accurately image biological events of interest. The design of smart NIR-II probes in response to specific biological targets or events could achieve excellent signal-to-background ratios.[136] There is no doubt that the development of smart NIR-II probes could facilitate the applications of NIR-II imaging in biomedicine.

Finally, as the limitations of NIR-II fluorescence fluorophores obstruct more extensive biomedical applications, auxiliary methods are necessary. Recently, non-invasive NIR-II imaging-guided surgery afforded benefits for solid tumor therapy, but still had a confined imaging penetration depth *in vivo*.[79,95] In clinical practice, for example, MRI and PET can enable identification of tumors in the whole body with unlimited penetration, and NIR-II fluorescence imaging has the ability to assure accurate delineation of tumor resection

margins. Therefore, the integration of NIR-II and other imaging modalities could offer a superior outcome, ultimately establishing a multimodal cancer detection and treatment method for precise surgery.[95] As intelligent NIR-II fluorescence imaging studies relevant to drug treatment are rarely reported, there is room for multifunctional NIR-II fluorophores to load drugs, creating responses to endogenetic substances at a high level and/or abnormal microenvironments in lesion sites which cannot be treated with surgery directly, and release drugs at targeted positions. The combination of imaging, localization and treatment of human diseases through multifunctional NIR-II fluorophores partly represents the future direction of NIR-II bioimaging.

Nevertheless, on the one hand, aiming to overcome biomedical imaging difficulties, advanced techniques and apparatuses with higher sensitivity and broader spectral ranges are indispensable to ensure the maximum exertion of the advantages engendered by NIR-II fluorescence imaging modalities. On the other hand, exploring the intrinsic favorable properties of the existing fluorophores, developing original fluorophores and realizing multifunctional imaging by means of artificial decorations are required for a promising and colorful NIR-II bioimaging.

Conflicts of interest

There are no conflicts to declare.

Acknowledgements

This work was partially supported by grants from the NSFC (21708012, 81600459, 51402099), 111 project B17019, NSFHP (2017CFB151, 2017CFA024, 2016CFB312), Self-determined research funds of CCNU from the colleges, basic research and operation of MOE (23020205170469) and Wuhan Morning Light Plan of Youth Science and Technology (201705304010321). Finally, we sincerely thank the referees for her/his critical reading of our manuscript, which helped to significantly improve our manuscript.

Notes and references

1 R. Weissleder, *Science*, 2006, **312**, 1168–1171.
2 J. M. Hoffman and S. S. Gambhir, *Radiology*, 2007, **244**, 39–47.
3 H. Chen, B. L. Dong, Y. H. Tang and W. Y. Lin, *Acc. Chem. Res.*, 2017, **50**, 1410–1422.
4 G. S. Hong, A. L. Antaris and H. J. Dai, *Nat. Biomed. Eng.*, 2017, **1**, 0010.
5 J. T. Hou, W. X. Ren, K. Li, J. Seo, A. Shama, X. Q. Yu and J. S. Kim, *Chem. Soc. Rev.*, 2017, **53**, 2076–2090.
6 L. Yuan, W. Y. Lin, K. B. Zheng, L. W. He and W. M. Huang, *Chem. Soc. Rev.*, 2013, **42**, 622–661.
7 Q. Q. Miao, C. Xie, X. Zhen, Y. Lyu, H. W. Duan, X. G. Liu, J. V. Jokerst and K. Y. Pu, *Nat. Biotechnol.*, 2017, **35**, 1102–1110.
8 F. Buckingham and V. Gouvemeur, *Chem. Sci.*, 2016, **7**, 1645–1652.
9 K. Y. Pu, A. J. Shuhendler, J. V. Jokerst, J. G. Mei, S. S. Gambhir, Z. N. Bao and J. H. Rao, *Nat. Nanotechnol.*, 2014, **9**, 233–239.
10 M. C. Heffern, L. M. Matosziuk and T. J. Meade, *Chem. Rev.*, 2014, **114**, 4496–4539.
11 F. Ding, S. Chen, W. S. Zhang, Y. F. Tu and Y. Sun, *Bioorg. Med. Chem.*, 2017, **25**, 5179–5184.
12 L. M. Nie and X. Y. Chen, *Chem. Sov. Rev.*, 2014, **43**, 7132–7170.
13 L. Manus, D. Masterone, E. A. Waters, X. Zhang, E. Schultz-Sikma, K. MacRenaris, D. Ho and T. J. Meade, *Nano Lett.*, 2010, **10**, 484–489.
14 D. J. Ye, A. Shuhendler, P. Pandit, K. Brewer, B. Rutt and J. H. Rao, *Chem. Sci.*, 2014, **5**, 3845–3852.
15 L. W. He, B. L. Dong, Y. Liu and W. Y. Lin, *Chem. Soc. Rev.*, 2016, **45**, 6449–6461.
16 Z. Yang, A. Sharma, J. Qi, X. Peng, D. Y. Lee, R. Hu, D. Lin, J. Qu and J. S. Kim, *Chem. Soc. Rev.*, 2016, **45**, 4651–4667.
17 X. H. Li, X. H. Gao, W. Shi and H. M. Ma, *Chem. Rev.*, 2014, **114**, 590–659.
18 Y. H. Tang, D. Y. Lee, J. L. Wang, G. H. Li, J. H. Yu, W. Y. Lin and J. Y. Yoon, *Chem. Soc. Rev.*, 2015, **44**, 5003–5015.
19 L. Yuan, W. Y. Lin, K. B. Zheng and A. S. Zhu, *Acc. Chem. Res.*, 2013, **46**, 1462–1473.
20 V. S. R. Harrison, C. E. Carney, K. W. MacRenaris, E. A. Waters and T. J. Meade, *J. Am. Chem. Soc.*, 2014, **137**, 9108–9116.
21 J. Liu, C. Chen, S. L. Ji, Q. Liu, D. Ding, D. Zhao and B. Liu, *Chem. Sci.*, 2017, **8**, 2782–2789.
22 Y. Sun, X. Ma, K. Cheng, B. Wu, J. Duan, H. Chen, L. Bu, R. Zhang, X. Hu, Z. Deng, L. Xing, X. Hong and Z. Cheng, *Angew. Chem., Int. Ed.*, 2015, **54**, 5981–5984.
23 Z. Yang, J. Cao, Y. He, J. Yang, T. Kim, X. Peng and J. S. Kim, *Chem. Soc. Rev.*, 2014, **43**, 4563–4601.
24 K. Y. Liu, X. Q. Kong, Y. Y. Ma and W. Y. Lin, *Angew. Chem., Int. Ed.*, 2017, **56**, 13489–13492.
25 B. L. Dong, X. Z. Song, X. Q. Kong, C. Wang, Y. H. Tang, Y. Liu and W. Y. Lin, *Adv. Mater.*, 2016, **28**, 8755–8759.
26 H. Chen, Y. H. Tang, M. G. Ren and W. Y. Lin, *Chem. Sci.*, 2016, **7**, 1896–1903.
27 A. L. Vahrmeijer, M. Hutteman, J. R. van der Vorst, C. J. H. van de Velde and J. V. Frangioni, *Nat. Rev. Clin. Oncol.*, 2013, **10**, 507–518.
28 C. A. Metildi, S. Kaushal, M. Pu, K. A. Messer, G. A. Luiken, A. R. Moossa, R. M. Hoffman and M. Bouvet, *Ann. Surg. Oncol.*, 2014, **21**, 1405–1411.
29 J. V. Frangioni, *Curr. Opin. Chem. Biol.*, 2003, **7**, 626–634.
30 A. Haque, M. H. Faizi, J. A. Rather and M. S. Khan, *Bioorg. Med. Chem.*, 2017, **25**, 2017–2034.
31 M. H. Lee, A. Sharma, M. J. Chang, J. Lee, S. Son, J. L. Sessler, C. Kang and J. S. Kim, *Chem. Soc. Rev.*, 2018, **47**, 28–52.
32 A. M. Smith, M. C. Mancini and S. Nie, *Nat. Nanotechnol.*, 2009, **4**, 710–711.

33 G. S. Hong, S. Diao, A. L. Antaris and H. J. Dai, *Chem. Rev.*, 2015, **115**, 10816–10906.
34 K. Welsher, Z. Liu, S. P. Sherlock, J. T. Bobinson, Z. Chen, D. Daranciang and H. J. Dai, *Nat. Nanotechnol.*, 2009, **4**, 773–780.
35 Z. M. Tao, G. S. Hong, C. Shinji, C. X. Chen, S. Diao, A. L. Antaris, B. Zhang, Y. P. Zou and H. J. Dai, *Angew. Chem., Int. Ed.*, 2013, **52**, 13002–13006.
36 A. L. Antaris, H. Chen, K. Cheng, Y. Sun, G. S. Hong, C. R. Qu, S. Diao, Z. X. Deng, X. M. Hu, B. Zhang, X. D. Zhang, O. K. Yaghi, Z. R. Alamparambil, X. C. Hong, Z. Cheng and H. J. Dai, *Nat. Mater.*, 2016, **15**, 235–242.
37 G. S. Hong, J. T. Robinson, Y. J. Zhang, S. Diao, A. L. Antaris, Q. B. Wang and H. J. Dai, *Angew. Chem., Int. Ed.*, 2012, **51**, 9818–9821.
38 Y. Zhang, G. S. Hong, Y. J. Zhang, G. C. Chen, F. Li, H. J. Dai and Q. B. Wang, *ACS Nano*, 2012, **6**, 3695–3702.
39 G. S. Hong, Y. P. Zhou, A. L. Antaris, S. Diao, D. Wu, K. Cheng, X. D. Zhang, C. X. Chen, B. Liu, Y. H. He, J. Z. Wu, J. Yuan, B. Zhang, Z. M. Tao, C. Fukunaga and H. J. Dai, *Nat. Commun.*, 2014, **5**, 4206.
40 D. Naczynski, M. Tan, M. Zevon, B. Wall, J. Kohl, A. Kulesa, S. Chen, C. Roth, R. Riman and P. Moghe, *Nat. Commun.*, 2013, **4**, 2199.
41 A. De La Zerda, *et al.*, *Nat. Nanotechnol.*, 2008, **3**, 557–562.
42 M. L. Schipper, N. Nakayama-Ratchford, C. R. Davis, N. W. S. Kam, P. Chu, Z. Liu, X. M. Sun, H. J. Dai and S. S. Gambhir, *Nat. Nanotechnol.*, 2008, **3**, 216–221.
43 Z. Liu, S. Tabakman, K. Welsher and H. J. Dai, *Nano Res.*, 2009, **2**, 85–120.
44 K. Ohkubo, N. Kohno, Y. Yamada and S. Fukuzumi, *Chem. Sci.*, 2015, **6**, 666–674.
45 G. S. Hong, J. C. Lee, A. Jha, S. Diao, K. H. Nakayama, L. Q. Hou, T. C. Doyle, J. T. Robinson, A. L. Antaris, H. J. Dai, J. P. Cooke and N. F. Huang, *Circ. Cardiovasc. Imaging*, 2014, **7**, 517–525.
46 M. J. O'Connell, *et al.*, *Science*, 2002, **297**, 593–596.
47 M. F. Islam, E. Rojas, D. M. Bergey, A. T. Johnson and A. G. Yodh, *Nano Lett.*, 2003, **3**, 269–273.
48 R. J. Chen, S. Bangsaruntip, K. A. Drouvalakis, N. W. S. Kam, M. Shim, Y. M. Li, W. Kim, P. J. Utz and H. J. Dai, *Proc. Nat. Acad. Sci. U.S.A.*, 2003, **100**, 4984–4989.
49 Z. Liu, S. M. Tabakman, Z. Chen and H. J. Dai, *Nat. Protoc.*, 2009, **4**, 1372–1382.
50 J. Chen, M. A. Hamon, H. Hu, Y. S. Chen, A. M. Rao, P. C. Eklund and R. C. Haddon, *Science*, 1998, **282**, 95–98.
51 N. W. S. Kam and H. J. Dai, *J. Am. Chem. Soc.*, 2005, **127**, 6021–6026.
52 J. Y. Zhao, D. Zhong and S. B. Zhou, *J. Mater. Chem. B.*, 2018, **6**, 349–365.
53 N. W. S. Kam, M. O. Connell, J. A. Wisdom and H. J. Dai, *Proc. Natl. Acad. Sci. U.S.A.*, 2005, **102**, 11600–11605.
54 H. Dumortier, S. Lacotte, G. Pastorin, R. Marega, W. Wu, D. Bonifazi, J. P. Briand, M. Prato, S. Muller and A. Bianco, *Nano Lett.*, 2006, **6**, 1522–1528.
55 P. Cherukuri, S. M. Bachilo, S. H. Litovsky and R. B. Weisman, *J. Am. Chem. Soc.*, 2004, **126**, 15638–15639.
56 P. Cherukuri, C. J. Gannon, T. K. Leeuw, H. K. Schmidt, R. E. Smalley, S. A. Curley and R. B. Weisman, *Proc. Natl. Acad. Sci. U.S.A.*, 2006, **103**, 18882–18886.
57 K. Welsher, Z. Liu, D. Daranciang and H. J. Dai, *Nano Lett.*, 2008, **8**, 586–590.
58 D. Ghosh, A. F. Bagley, Y. J. Na, M. J. Birrer, S. N. Bhatia and A. M. Belcher, *Proc. Natl. Acad. Sci. U.S.A.*, 2014, **111**, 13948–13953.
59 E. M. C. Hillman and A. Moore, *Nat. Photonics*, 2007, **1**, 526–530.
60 J. T. Robinson, K. Welsher, S. M. Tabakman, S. P. Sherlock, H. L. Wang, R. Luong and H. J. Dai, *Nano Res.*, 2010, **3**, 779–793.
61 A. L. Antaris, J. T. Robinson, O. K. Yaghi, G. S. Hong, B. Zhang and H. J. Dai, *ACS Nano*, 2013, **7**, 3644–3652.
62 S. Diao, J. L. Blackburn, G. S. Hong, A. L. Antaris, J. L. Chang, J. Z. Wu, B. Zhang, K. Cheng, C. J. Kuo and H. J. Dai, *Angew. Chem., Int. Ed.*, 2015, **54**, 14758–14762.
63 G. S. Hong, S. Diao, J. L. Chang, A. L. Antaris, C. X. Chen, B. Zhang, S. Zhao, D. N. Atochin, P. L. Huang, K. I. Andreasson, C. J. Kuo and H. J. Dai, *Nat. Photonics*, 2014, **8**, 723–730.
64 H. Gong, R. Peng and Z. Liu, *Adv. Drug. Deliv. Rev*, 2013, **65**, 1951–1963.
65 S. Ghosh, S. M. Bachilo and R. B. Weisman, *Nat. Nanotechnol.*, 2010, **5**, 443–450.
66 X. M. Tu, S. Manohar, A. Jagota and M. Zheng, *Nature*, 2009, **460**, 250–253.
67 Y. Miyata, K. Shiozawa, Y. Asada, Y. Ohno, R. Kitaura, T. Mizutani and H. Shinohara, *Nano Res.*, 2011, **4**, 963–970.
68 K. Moshammer, F. Hennrich and M. M. Kappes, *Nano Res.*, 2009, **2**, 599–606.
69 Y. Zhang, Y. Zhang, G. Hong, W. He, K. Zhou, K. Yang, F. Li, G. Chen, Z. Liu, H. Dai and Q. Wang, *Biomaterials*, 2013, **34**, 3639–3646.
70 A. Louie, *Chem. Rev.*, 2010, **110**, 3146–3195.
71 E. D. Cosco, J. R. Caram, O. T. Bruns, D. Franke, R. A. Day, E. P. Farr, M. G. Bawendi and E. M. Sletten, *Angew. Chem., Int. Ed.*, 2017, **56**, 13126–13129.
72 M. J. Schnermann, *Nature*, 2017, **551**, 176–177.
73 B. H. Li, L. F. Lu, M. Y. Zhao, H. L. Zu and F. Zhang, *Angew. Chem., Int. Ed.*, 2018, DOI: 10.1002/anie.201801226.
74 G. Qian and Z. Y. Wang, *Chem.–Asian J.*, 2010, **5**, 1006–1029.
75 G. Qian, J. P. Gao and Z. Y. Wang, *Chem. Commun.*, 2012, **48**, 6426–6428.
76 G. Qian, Z. Zhong, M. Luo, D. B. Yu, Z. Q. Zhang, Z. Y. Wang and D. G. Ma, *Adv. Mater.*, 2009, **21**, 111–116.
77 Y. Sun, C. R. Qu, H. Chen, M. M. He, C. Tang, K. Q. Shou, S. Hong, M. Yang, Y. X. Jiang, B. B. Ding, Y. L. Xiao, L. Xing, X. C. Hong and Z. Cheng, *Chem. Sci.*, 2016, **7**, 6203–6207.
78 Y. Sun, M. M. Ding, X. D. Zeng, Y. L. Xiao, H. P. Wu, H. Zhou, B. B. Ding, C. R. Qu, W. Hou, A. Er-bu, Y. J. Zhang, Z. Cheng and X. C. Hong, *Chem. Sci.*, 2017, **8**, 3489–3493.
79 K. Q. Shou, C. R. Qu, Y. Sun, H. Chen, S. Chen, L. Zhang, H. B. Xu, X. C. Hong, A. X. Yu and Z. Cheng, *Adv. Funct. Mater.*, 2017, **27**, 1700995.
80 Y. Feng, *et al.*, *Chem. Sci.*, 2017, **8**, 3703–3711.

81 S. Singha, D. Kim, B. Roy, S. Sambasivan, H. Moon, A. S. Rao, J. Y. Kim, T. Joo, J. W. Park and Y. M. Rhee, *Chem. Sci.*, 2015, **6**, 4335–4342.
82 Q. L. Yang, Z. R. Ma, H. Wang, B. Zhou, S. J. Zhu, Y. T. Zhong, J. Y. Wang, H. Wan, A. L. Antaris, R. Ma, X. Zhang, J. Y. Yang, X. D. Zhang, H. T. Sun, W. Q. Liu, Y. Y. Liang and H. J. Dai, *Adv. Mater.*, 2017, **29**, 1605497.
83 X. D. Zhang, H. Wang, A. L. Antaris, L. I. Li, S. Diao, R. Ma, A. Nguyen, G. S. Hong, Z. R. Ma, J. Wang, S. J. Zhu, J. M. Castellano, T. Wyss-Coray, Y. Y. Liang, J. Luo and H. J. Dai, *Adv. Mater.*, 2016, **28**, 6872–6879.
84 S. Zhu, Q. L. Yang, A. L. Antaris, J. Y. Yue, Z. R. Ma, H. Wang, W. Huang, H. Wan, J. Wang, S. Diao, B. Zhang, X. Y. Li, Y. T. Zhong, K. Yu, G. S. Hong, J. Luo, Y. Y. Liang and H. J. Dai, *Proc. Natl. Acad. Sci. U.S.A.*, 2017, **114**, 962–967.
85 D. Yang, H. S. Wang, C. J. Sun, H. Zhao, K. Hu, W. R. Qin, R. Ma, F. Ying, X. Qin, Q. L. Zhang, Y. Y. Liang and Z. G. Li, *Chem. Sci.*, 2017, **8**, 6322–6326.
86 Q. L. Yang, Z. B. Hu, S. J. Zhu, R. Ma, H. L. Ma, Z. R. Ma, H. Wan, T. Zhu, Z. Y. Jiang, W. Q. Liu, L. Y. Jiao, H. T. Sun, Y. Y. Liang and H. J. Dai, *J. Am. Chem. Soc.*, 2018, **140**, 1715–1724.
87 S. Zhu, S. Herraiz, J. Yue, M. Zhang, H. Wan, Q. Yang, Z. Ma, Y. Wang, J. He, A. L. Antaris, Y. Zhong, S. Diao, Y. Feng, Y. Zhou, K. Yu, G. Hong, Y. Liang, A. J. Hsueh and H. Dai, *Adv. Mater.*, 2018, **30**, 1705799.
88 Z. Starosolski, R. Bhavane, K. B. Ghaghada, S. A. Vasudevan, A. Kaay and A. Annapragada, *PLoS One*, 2017, **12**, e0187563.
89 J. A. Carr, D. Franke, J. R. Caram, C. F. Perkinson, V. Askoxylakis, M. Datta, D. Fukumura, R. K. Jain, M. G. Bawendi and O. T. Bruns, *bioRxiv*, 2017, DOI: 10.1101/100768.
90 C. A. Metildi, S. Kaushal, C. S. Snyder, R. M. Hoffman and M. Bouvet, *J. Surg. Res.*, 2013, **179**, 87–93.
91 R. M. Hoffman, *Nat. Rev. Cancer*, 2015, **15**, 451–452.
92 T. Murakami, Y. Hiroshima, Y. Zhang, M. Bouvet, T. Chishima, K. Tanaka, I. Endo and R. M. Hoffman, *J. Surg. Oncol.*, 2015, **112**, 119–124.
93 T. Nakamura, F. Sugihara, H. Matsushita, Y. Yoshioka, S. Mizukamiab and K. Kikuchi, *Chem. Sci.*, 2015, **6**, 1986–1990.
94 Y. Sun, *et al.*, *Angew. Chem., Int. Ed.*, 2015, **54**, 5981–5984.
95 Y. Sun, *et al.*, *Chem. Sci.*, 2018, **9**, 2092–2097.
96 E. Petryayeva, W. R. Algar and I. L. Medintz, *Appl. Spectrosc.*, 2013, **67**, 215–252.
97 I. Medintz, H. T. Uyeda, E. Goldman and H. Mattoussi, *Nat. Mater.*, 2005, **4**, 435–446.
98 Y. P. Gu, R. Cui, Z. L. Zhang, Z. X. Xieand and D. W. Pang, *J. Am. Chem. Soc.*, 2012, **134**, 79–82.
99 Y. Nakane, Y. Tsukasaki, T. Sakata, H. Yasuda and T. Jin, *Chem. Commun.*, 2013, **49**, 7584–7586.
100 C. Ou, *et al.*, *Nat. Mater.*, 2013, **12**, 445–451.
101 R. J. Cui, A. J. Wan, X. F. Liu, W. Yuan and H. Jin, *Nanoscale*, 2014, **6**, 5467–5473.
102 C. Y. Li, Y. J. Zhang, M. Wang, Y. Zhang, G. C. Chen, L. Li, D. M. Wu and Q. B. Wang, *Biomaterials*, 2014, **35**, 393–400.
103 G. C. Chen, F. Tian, Y. Zhang, Y. J. Zhang, C. Y. Li and Q. B. Wang, *Adv. Funct. Mater.*, 2014, **24**, 2481–2488.
104 G. C. Chen, F. Tian, C. Y. Li, Y. J. Zhang, Z. Weng, Y. Zhang, R. Peng and Q. B. Wang, *Biomaterials*, 2015, **53**, 265–273.
105 C. Y. Li, F. Li, Y. J. Zhang, W. J. Zhang, X. E. Zhang and Q. B. Wang, *ACS Nano*, 2015, **9**, 12255–12263.
106 Y. F. Kong, J. Chen, H. W. Fang, G. Heath, Y. Wo, W. L. Wang, Y. X. Li, Y. Guo, S. Evans, S. Y. Chen and D. J. Zhou, *Chem. Mater.*, 2016, **28**, 3041–3050.
107 Y. Tsukasaki, M. Morimatsu, G. Nishimura, T. Sakata, H. Yasuda, A. Komatsuzaki, T. M. Watanabe and T. Jin, *RSC Adv.*, 2014, **4**, 41146–41171.
108 A. Zebibula, N. Alifu, L. Xia, C. Sun, X. Yu, D. Xue, L. Liu, G. Li and J. Qian, *Adv. Funct. Mater.*, 2018, **28**, 1703451.
109 O. T. Bruns, *et al.*, *Nat. Biomed. Eng.*, 2017, **1**, 0056.
110 Y. Y. Jiang, P. K. Upputuri, C. Xie, Y. Lyu, L. L. Zhang, Q. H. Xiong, M. Pramanik and K. Y. Pu, *Nano Lett.*, 2017, **17**, 4964–4969.
111 J. C. Li, J. H. Rao and K. Y. Pu, *Biomaterials*, 2018, **155**, 217–235.
112 J. J. Zhou, Y. Y. Jiang, S. Hou, P. K. Upputuri, D. Wu, J. C. Li, P. Wang, X. Zhen, M. Pramanik, K. Y. Pu and H. W. Duan, *ACS Nano*, 2018, **12**, 2643–2651.
113 J. Lee, A. J. Kalin, T. Y. Yuan, M. Al-Hashimiand and L. Fang, *Chem. Sci.*, 2017, **8**, 2503–2521.
114 S. L. Fronk, M. Wang, M. Ford, J. Coughlin, C. K. Ma and G. C. Bazan, *Chem. Sci.*, 2016, **7**, 5313–5321.
115 J. Cornil, I. Gueli, A. Dkhissi, J. C. Sancho-Garcia, E. Hennebicq, J. P. Calbert, V. Lemaur, D. Beljonne and J. L. Brédas, *J. Chem. Phys.*, 2003, **118**, 6615–6623.
116 Y. Wang, Q. Peng, Q. Hou, K. Zhao, Y. Liang and B. Li, *Theor. Chem. Acc.*, 2011, **129**, 257–270.
117 K. Q. Shou, Y. F. Tang, H. Chen, S. Chen, L. Zhang, A. Zhang, Q. L. Fan, A. X. Yuand and Z. Cheng, *Chem. Sci.*, 2018, **9**, 3105–3110.
118 D. Yang, *et al*, *Chem. Soc. Rev.*, 2015, **44**, 1416–1448.
119 F. Wang, *et al*, *Nat. Mater.*, 2011, **10**, 968–973.
120 X. Y. Jiang, C. Cao, W. Feng and F. Y. Li, *J. Mater. Chem. B.*, 2016, **4**, 87–95.
121 M. Yu, *et al*, *Anal. Chem.*, 2009, **81**, 930–935.
122 G. S. Yi and G. M. Chow, *Chem. Mater.*, 2007, **19**, 341–343.
123 B. F. Moore, *et al*, *J. Am. Chem. Soc.*, 2011, **133**, 373–378.
124 A. Kornienko, B. F. Moore, G. A. Kumar, M. C. Tan, R. E. Riman, M. G. Brik, T. J. Emge and J. G. Brennan, *Inorg. Chem.*, 2011, **50**, 9184–9190.
125 M. C. Tan, D. J. Naczynski, P. V. Moghe and R. E. Riman, *Aust. J. Chem.*, 2013, **66**, 1008–1020.
126 J. V. Frangioni, *Curr. Opin. Chem. Biol.*, 2003, **7**, 626–634.
127 M. C. Tan, *et al*, *J. Appl. Phys.*, 2009, **106**, 063118.
128 R. Wang, X. Li, L. Zhou and F. Zhang, *Angew. Chem., Int. Ed.*, 2014, **53**, 12086–12090.
129 D. J. Naczynski, *et al*, *Nat. Commun.*, 2013, **4**, 2199.
130 U. Rocha, *et al*, *Small*, 2014, **10**, 1141–1154.
131 V. P. Gapontsev, A. A. Izyneev, Y. E. Sverchkov and M. Syrtlanov, *Quantum Electron.*, 1981, **11**, 1101–1103.
132 Y. T. Zhong, *et al*, *Nat. Commun.*, 2017, **8**, 737.

133 Y. Y. Jiang, J. C. Li, X. Zhen, C. Xieand and K. Y. Pu, *Adv. Mater.*, 2018, **30**, 1705980.
134 A. Zebihula, N. Alifu, L. Q. Xia, C. W. Sun, X. M. Yu, D. W. Xue, L. W. Liu, G. H. Li and J. Qian, *Adv. Funct. Mater.*, 2018, **28**, 1703451.
135 J. Qi, C. W. Sun, A. Zebibula, H. Q. Zhang, R. K. Kwok, X. Y. Zhao, W. Xi, J. Y. Lam, J. Qian and B. Z. Tang, *Adv. Mater.*, 2018, **30**, 1706856.
136 G. Xu, Q. L. Yan, X. G. Lv, Y. Zhu, K. Xin, B. Shi, R. C. Wang, J. Chen, W. Gao, P. Shi, C. H. Fan, C. C. Zhao and H. Tian, *Angew. Chem., Int. Ed.*, 2018, **57**, 3626–3630.